Canadian Geotechnical Journal

Article

Surficial liquefaction manifestation severity thresholds for profiles having high fines-content, high-plasticity soils

Sneha Upadhyaya[a], Brett W. Maurer[b], Russell A. Green[a], Adrian Rodriguez-Marek[a], and Sjoerd van Ballegooy[c]

[a]Department of Civil and Environmental Engineering, Virginia Tech, Blacksburg, VA 24061, USA; [b]Department of Civil and Environmental Engineering, University of Washington, Seattle, WA 98195, USA; [c]Geotechnical, Tonkin + Taylor Ltd., 105 Carlton Gore Rd., Newmarket, Auckland 1023, New Zealand

Corresponding author: **Russell A. Green** (email: rugreen@vt.edu)

Abstract

The severity of surficial liquefaction manifestation was significantly over-predicted for a large subset of case histories from relatively recent earthquakes that impacted the Canterbury region of New Zealand. Such over-predicts generally occurred for profiles having predominantly high fines-content (FC), high-plasticity soil strata. Herein, the liquefaction case histories from the Canterbury earthquakes are used to investigate the performances of three different manifestation severity index (MSI) models. The prevalence of high FC, high-plasticity strata in a profile is quantified through the soil behavior type index averaged over the upper 10 m of a profile (I_{c10}). It is shown that for each MSI model (1) the threshold MSI value distinguishing cases with and without manifestation increases as I_{c10} increases and (2) the ability of the MSI to segregate cases with and without manifestation decreases with increasing I_{c10}. Additionally, probabilistic models are proposed for evaluating the severity of surficial liquefaction manifestation as a function of MSI and I_{c10}. The approaches presented in this study allow better interpretations of predictions made by existing MSI models, although their efficacy decreases at sites with high I_{c10}. An improved MSI model is ultimately needed that better accounts for the effects of high-FC, high-plasticity soils more directly.

Key words: liquefaction, earthquake, manifestation severity index, Canterbury earthquakes

Introduction

The objective of this study is to investigate the effect of high fines-content (FC), high-plasticity soils on the prediction of the occurrence and severity of surficial liquefaction manifestations at free-field sites, which has been shown to correlate to liquefaction damage potential for near-surface infrastructure at developed sites (e.g., Iwasaki et al. 1978). Towards this end, the predictive performance of three existing manifestation severity index (MSI) models [i.e., liquefaction potential index (LPI), Ishihara-inspired LPI (LPI_{Ish}), and liquefaction severity number (LSN)] is investigated as a function of the cone penetration test (CPT) soil behavior type index (I_c) averaged over the upper 10 m of the soil profile (I_{c10}), wherein I_{c10} is used to infer the amount of high-FC, high-plasticity strata in the profile. Specifically, manifestation severity thresholds for distinguishing cases with different manifestation severities (e.g., cases with and without manifestation) for each MSI model considered herein are evaluated as a function of I_{c10}. Additionally, probabilistic models are proposed to evaluate the severity of surficial liquefaction manifestation as a function of the computed MSI and I_{c10}.

The M_w7.1 September 2010 Darfield earthquake, the M_w6.2 February 2011 Christchurch earthquake, and the M_w5.7 February 2016 Valentine's Day earthquake, collectively referred to herein as the Canterbury earthquakes (CEs), resulted in widespread liquefaction that caused extensive damage to infrastructure throughout the city of Christchurch and its surroundings (e.g., Cubrinovski and Green 2010; Cubrinovski et al. 2011; Green et al. 2011*a*, *b*, 2014; Maurer et al. 2014; van Ballegooy et al. 2014*b*). While the Canterbury region of New Zealand was impacted by more than ten relatively recent earthquakes that triggered liquefaction (Quigley et al. 2013), the M_w7.1, 4 September 2010 Darfield; the M_w6.2, 22 February 2011 Christchurch; and the M_w5.7 Valentine's Day earthquakes were the most notable in terms of the well-documented spatial extent and the severity of liquefaction damage. The ground motions from these earthquakes were recorded by a large network of strong motion stations in the area (Bradley and Cubrinovski 2011; Bradley 2012). Following the 2010 Darfield event, an extensive geotechnical site characterization program was initiated in Christchurch and its environs, the majority of which was funded by the New Zealand Earthquake Commission (EQC), resulting in more than 35 000 CPT soundings performed to date. Additionally, the ground surface observations were well documented via post-earthquake ground reconnaissance and high-resolution aerial photos and satellite imagery. All of this data are stored in the New Zealand Geotechnical Database (NZGD 2016), an online repository available for use by researchers and practitioners. This unprecedented quantity of

data has been utilized by multiple studies to investigate the accuracies of various procedures that predict liquefaction triggering and the resulting severity of surficial liquefaction manifestations (e.g., Green et al. 2014; 2015; Maurer et al. 2014, 2015*b*, *c*; van Ballegooy et al. 2012, 2014*b*, 2015). These studies have shown that while existing procedures are generally effective in predicting the liquefaction response, the severity of manifestation was systematically over-predicted for a non-trivial number of sites. For example, Maurer et al. (2014) shows that the LPI framework is relatively accurate in predicting the severity of surficial liquefaction manifestations in eastern Christchurch but "excessively" over-predicted the severity in western Christchurch.

Such over-predictions may be attributed to several factors associated with the uncertainties in site characterization and in the procedures that predict liquefaction triggering and the severity of manifestations (e.g., Boulanger et al. 2016; Yost et al. 2021, 2022). Predominant factors include the presence of a thick non-liquefiable crust and (or) interbedded non-liquefiable soils high in FC and plasticity (e.g., Maurer et al. 2014, 2015*a*, *b*; Green et al. 2018). In particular, the presence of plastic soils with low permeability can affect the generation and redistribution of excess pore pressure within a soil profile, potentially suppressing surface manifestation of the liquefied soils (e.g., Ozutsumi et al. 2002; Juang et al. 2005; Jia and Wang 2012; Maurer et al. 2015*b*; Beyzaei et al. 2018; Cubrinovski et al. 2019). In this regard, proposed manifestation severity thresholds specific to different MSI models have been found to be less applicable at sites with predominantly silty or clayey soils. For example, Lee et al. (2003) used LPI to analyze case histories from the 1999 chi-Chi (Taiwan) earthquake, mainly comprising sites with silty sands and sandy silt strata, and proposed that a threshold LPI of 13 be used to distinguish between sites with and without manifestations of liquefaction (in contrast to LPI = 5 threshold originally proposed by Iwasaki et al. 1978). Similarly, Maurer et al. (2015*b*) analyzed some of the CE case histories and found the threshold LPI value to be significantly higher at sites with predominantly silty and clayey soil mixtures than at sites with predominantly clean sands or silty sands. Maurer et al. (2015*b*) made this distinction using I_{c10} to parse sites into those comprising predominantly clean sands or silty sands ($I_{c10} < 2.05$) and those comprising predominantly silty or clayey soil mixtures ($I_{c10} \geq 2.05$). They found that sites with $I_{c10} < 2.05$ had an optimum threshold LPI for distinguishing sites with and without manifestation of 4.9, whereas sites with $I_{c10} \geq 2.05$ had an optimum threshold LPI of 13. The findings from these studies indicate that the relationship between the computed MSI and the severity of surficial liquefaction manifestation is dependent on the extent to which a soil profile contains high-FC, high-plasticity soil strata.

This study rigorously investigates the effects of high-FC, high-plasticity soils on the predictive performance of three existing MSI models using empirical liquefaction case histories resulting from three of the relatively recent earthquakes that have impacted the Canterbury region of New Zealand. Using an approach similar to that of Maurer et al. (2015*b*), this study uses I_{c10} to parse soil profiles by their average inferred soil type but considers multiple finer bins of I_{c10} to study the influence of I_{c10} on the predictive performance of MSI models with greater resolution. Specifically, receiver operating characteristic (ROC) analyses are performed to investigate the optimum MSI thresholds specific to LPI, LPI_{Ish}, and LSN models, as well as their predictive efficacies, as a function of I_{c10}. Additionally, using logistic regression, probabilistic models are proposed for predicting the severity of manifestation as a function of MSI and I_{c10}. In the following, overviews of the LPI, LPI_{Ish}, and LSN models are presented, which is followed by a summary of the liquefaction case-history data set and the methodologies used to analyze them, to include an overview of ROC analysis. Finally, the results are presented and discussed in detail.

Overview of existing manifestation severity index models

Liquefaction potential index

The LPI proposed by Iwasaki et al. (1978) is commonly used to predict the severity of the surficial liquefaction manifestation:

$$\text{LPI} = \int_0^{z_{max}} F\,(\text{FS}) \cdot w\,(z)\,\mathrm{d}z \tag{1}$$

where FS is the factor of safety against liquefaction triggering, computed using a liquefaction triggering model; z is depth below the ground surface in meters; z_{max} is the maximum depth considered, generally taken as 20 m; and F(FS) and $w(z)$ are functions that account for the weighted contributions of FS and z to the severity of surficial liquefaction manifestation. Specifically, $F(\text{FS}) = 1 - \text{FS}$ for $\text{FS} \leq 1$ and $F(\text{FS}) = 0$ otherwise, and $w(z) = 10–0.5z$. Thus, LPI assumes that the severity of surface manifestation depends on the cumulative thickness of liquefied soil layers, the proximity of those layers to the ground surface, and the amount by which FS in each layer is less than 1.0. Given this definition, LPI can range from zero to 100. Analyzing the standard penetration test data from 55 sites in Japan, Iwasaki et al. (1978) proposed that severe liquefaction is expected for sites where LPI > 15 but not where LPI < 5. This criterion, defined by two threshold values of LPI, is commonly referred to as "Iwasaki Criterion". In today's practice, LPI = 5 is commonly used as a deterministic threshold for predicting surficial liquefaction manifestation, such that some degree of manifestation is expected where LPI > 5, but no manifestation is expected where LPI < 5.

Ishihara-inspired liquefaction potential index

Maurer et al. (2015*a*) proposed modifications to LPI to account for the influence of non-liquefied crust thickness on the severity of surficial liquefaction manifestations using the relationship proposed by Ishihara (1985), which relates the thicknesses of the non-liquefiable crust (H_1) and the liquefied stratum (H_2) to the occurrence of surficial liquefaction manifestation. The modified LPI was termed LPI_{Ish} and is defined

as (Maurer et al. 2015*a*)

$$\text{(2a)}\quad \text{LPI}_{\text{Ish}} = \int_{H_1}^{z_{\max}} F(\text{FS}) \cdot \frac{25.56}{z} \cdot \text{d}z$$

where

$$\text{(2b)}\quad F(\text{FS}) = \begin{cases} 1 - \text{FS if FS} \le 1 \cap H_1 \cdot m(\text{FS}) \le 3 \\ 0 \quad \text{otherwise} \end{cases}$$

and

$$\text{(2c)}\quad m(\text{FS}) = \exp\left(\frac{5}{25.56\,(1-\text{FS})}\right) - 1;\, m(\text{FS} > 0.95) = 100$$

where z, FS, and $z_{\max}$ are as defined previously for LPI (eq. 1). As can be surmised from eq. 2*a*, the LPI_{Ish} framework accounts for the relative thicknesses of H_1 and H_2 by imposing an additional constraint on F(FS). Additionally, LPI_{Ish} uses a power-law depth-weighting function, consistent with Ishihara's boundary curves, which results in LPI_{Ish} giving a higher weight to shallower layers than LPI in predicting the severity of surficial manifestations.

Liquefaction severity number

Liquefaction severity number (LSN) was proposed by van Ballegooy et al. (2012, 2014*b*) and uses post-liquefaction volumetric strain (ε_v) as an index to account for the influence of contractive and dilative tendencies of soils at moderate to large strains on the severity of surficial manifestation. LSN is given by

$$\text{(3)}\quad \text{LSN} = \int_0^{z_{max}} 1000 \cdot \frac{\varepsilon_v}{z} \text{d}z$$

where z and $z_{\max}$ are as defined previously for LPI and LPI_{Ish} (eqs. 1 and 2*a*). $z_{\max}$ is generally taken as 10 m for LSN; however, this study uses 20 m. ε_v can be estimated as a function of the relative density (D_r) of the soil and FS using the relationships originally proposed by Ishihara and Yoshimine (1992) and later modified by Zhang et al. (2002) to express ε_v as a function of normalized cone tip resistance (q_{c1Ncs}) and FS. Similar to LPI_{Ish}, LSN also uses a power-law depth-weighting function.

Data and methodology

Canterbury earthquakes liquefaction case histories

This study utilizes about 3 800 CPT soundings from sites where the severities of surficial manifestation were well documented after at least one of the following earthquakes: the M_w7.1 September 2010 Darfield earthquake, the M_w6.2 February 2011 Christchurch earthquake, and the M_w5.7 February 2016 Valentine's Day earthquake (i.e., the CEs). The CPT soundings were selected to provide a spatial representation of soil profiles across Christchurch and a balance among different severities of surficial liquefaction manifestations. A map showing the spatial distributions of the CPT sounding locations used in this study is shown in Fig. 1, and Table S1 in the electronic supplement provides additional details about the case histories. Furthermore, a detailed description of the quality-control criteria used in compiling these CPT soundings is provided in Maurer et al. (2014, 2015*b*) and Geyin et al. (2021). Cases where the predominant form of manifestation was lateral spreading were excluded from the analyses, since none of the MSI models considered in this study account for the factors governing the occurrence and severity of lateral spreading. For all other cases, the severity of manifestation was classified as either "No Liquefaction", "Marginal", "Moderate", or "Severe" following the Green et al. (2014) criteria.

As implied by the naming scheme, "No Liquefaction" includes all the cases where no liquefaction surface manifestations were observed, "Minor Liquefaction" includes all the cases where minor surficial liquefaction manifestations were observed, etc. Table 1 provides quantitative metrics for the severity categorization used herein (Green et al. 2014). However, because the severity of surficial liquefaction manifestations is a continuum ranging from none to very severe, any sort of discrete categorization of "Minor", "Moderate", and "Severe" is inherently subjective, regardless of the best efforts to quantify liquefaction severity. As a result, the reader is directed to Green et al. (2014), which gives examples of high-resolution aerial images of the different severity manifestation categories to help reduce ambiguity in how the authors classified the case histories. With all these considerations, 9 631 high-quality case histories were used in further analyses in this study.

Fig. 1. Map of spatial distributions of CPT sounding locations from CEs (Google Satellite imagery, base image data© 2022 Google).

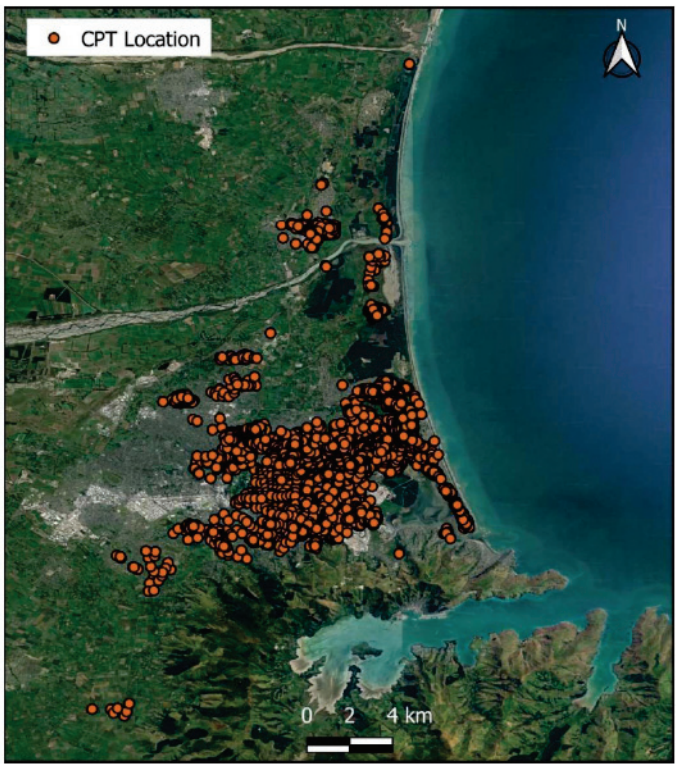

Table 1. Liquefaction severity classification criteria (after Green et al. 2014).

Classification	Criteria
No liquefaction	No surficial liquefaction manifestation or lateral spread cracking
Minor liquefaction	Small, isolated liquefaction features; streets had traces of ejecta or wet patches less than a vehicle width; <5% of ground surface covered by ejecta
Moderate liquefaction	Groups of liquefaction features; streets had ejecta patches greater than a vehicle width but were still passable; 5%–40% of ground surface covered by ejecta
Severe liquefaction	Large masses of adjoining liquefaction features; streets impassible due to liquefaction; >40% of ground surface covered by ejecta

Peak ground accelerations (PGAs) are required to estimate the seismic demand at the case-history sites. In prior CE studies (e.g., Green et al. 2014; Maurer et al. 2014, 2015*b*, *c*, *d*, 2017*a*, 2017*b*, 2019; van Ballegooy et al. 2015; Upadhyaya et al. 2018; among others), PGAs were obtained using the Bradley (2013*b*) procedure, which combines the unconditional PGA distributions as estimated by the Bradley (2013*a*) ground motion prediction equation, the actual recorded PGAs at the strong motion stations (SMSs), and the spatial correlation model of Goda and Hong (2008), to compute the conditional PGAs at the sites of interest. However, the PGAs at four SMSs during the M_w6.2 February 2011 Christchurch earthquake were inferred to be associated with high-frequency dilation spikes as a result of liquefaction triggering in the soil profiles at the stations and were higher than the pre-liquefaction PGAs (e.g., Wotherspoon et al. 2014, 2015). Such artificially high PGAs at the liquefied SMSs can result in over-estimated PGAs at the nearby case-history sites (hence, overly conservative seismic demand), which in turn can lead to over-predictions of the severity of surficial liquefaction manifestations (Upadhyaya et al. 2019*a*). Accordingly, in the present study, pre-liquefaction PGAs at the four liquefied SMSs were used to estimate PGAs at the case-history locations for the 2011 Christchurch earthquake. Note that for the 2010 Darfield and 2016 Valentine's Day earthquakes, previously estimated PGAs remain unchanged.

Accurate estimation of ground-water table (GWT) depth is critical to evaluating liquefaction triggering and the resulting severity of surficial manifestations (e.g., Chung and Rogers 2011; Maurer et al. 2014). The GWT depth at each case-history site immediately prior to the earthquake was estimated using the robust, event-specific regional ground-water models of van Ballegooy et al. (2014*a*), as in prior CE studies (e.g., Maurer et al. 2014; 2015*b*, *c*, *d*; 2017*a*, *b*; 2019; van Ballegooy et al. 2015; Upadhyaya et al. 2018; 2022; among others). Due to seasonal ground-water fluctuations, these GWT depths may differ from the GWT depths determined from the pore water pressure transducer measurements immediately behind the cone tip (i.e., u2) at the time that the CPT soundings were performed, where the latter GWT depths were used for CPT stress normalization as a part of sounding data processing.

Evaluation of liquefaction triggering and severity of surficial liquefaction manifestation

Factor of safety (FS) against liquefaction is used as a primary input in computing LPI, LPI_{Ish}, and LSN. In this study, FS was computed using the deterministic liquefaction-triggering model of Boulanger and Idriss (2014). Inherent to this process, an I_c cutoff value of 2.5 was used to distinguish between liquefiable and non-liquefiable soils, such that soils with $I_c > 2.5$ were considered to be non-liquefiable (Maurer et al. 2017*b*, 2019). Moreover, the FC was estimated using the Christchurch-specific I_c–FC correlation proposed by Maurer et al. (2019). Finally, for each of the 9 631 case histories considered in this study, LPI, LPI_{Ish}, and LSN values were computed using eqs. 1, 2, and 3, respectively.

Receiver operating characteristic analyses

To investigate the influence of high-FC, high-plasticity soils on the predictive performance of each MSI model considered in this study, the CE case histories were divided into multiple subsets on the basis of I_{c10}. As stated previously, I_{c10} is used herein to infer the extent to which a profile contains high-FC, high-plasticity soils. The use of I_c for inferring soil type was first proposed by Jeffries and Davies (1993) and then modified and popularized by Robertson and Wride (1998). Using CPT data and lab tests on samples from parallel borings, Maurer et al. (2017*b*, 2019) confirmed the suitability of using I_c to infer FC and soil type within the CE study area. ROC analyses (e.g., Fawcett 2005) were then performed on each I_{c10} subset to evaluate: (1) the optimum threshold MSI values for distinguishing cases with and without manifestation and (2) the predictive efficacy of the MSI model, as a function of I_{c10}. An overview of the ROC analysis is presented in the following section.

Overview of ROC analysis

ROC analyses have been widely used to evaluate the performance of diagnostic models, including extensive use in medical diagnostics (e.g., Zou 2007) and to a much lesser degree in geotechnical engineering (e.g., Oommen et al. 2010; Maurer et al. 2015*b*, *c*, *d*, 2017*a*, *b*, 2019; Green et al. 2017; Zhu et al. 2017; Upadhyaya et al. 2018, 2019*b*, 2022; Yost et al. 2021). In particular, in cases where the distribution of "positives" (e.g., cases of observed surficial liquefaction manifestation) and "negatives" (e.g., cases of no observed surficial liquefaction manifestations) overlap, ROC analyses can be used (1) to identify the optimum diagnostic threshold (e.g., MSI thresholds) for distinguishing between the positives and negatives and (2) to assess the relative efficacies of competing diagnostic models, independent of the thresholds used. The primary focus of this paper is on (1).

An ROC curve is a plot of the true positive rate (R_{TP}) (i.e., surficial liquefaction manifestation was observed as predicted)

Fig. 2. Conceptual illustration of ROC analyses: (*a*) frequency distributions of surficial liquefaction manifestation and no surficial liquefaction manifestation observations as a function of LPI and (*b*) the corresponding ROC curve (after Maurer et al. 2015*b*, *c*, *d*).

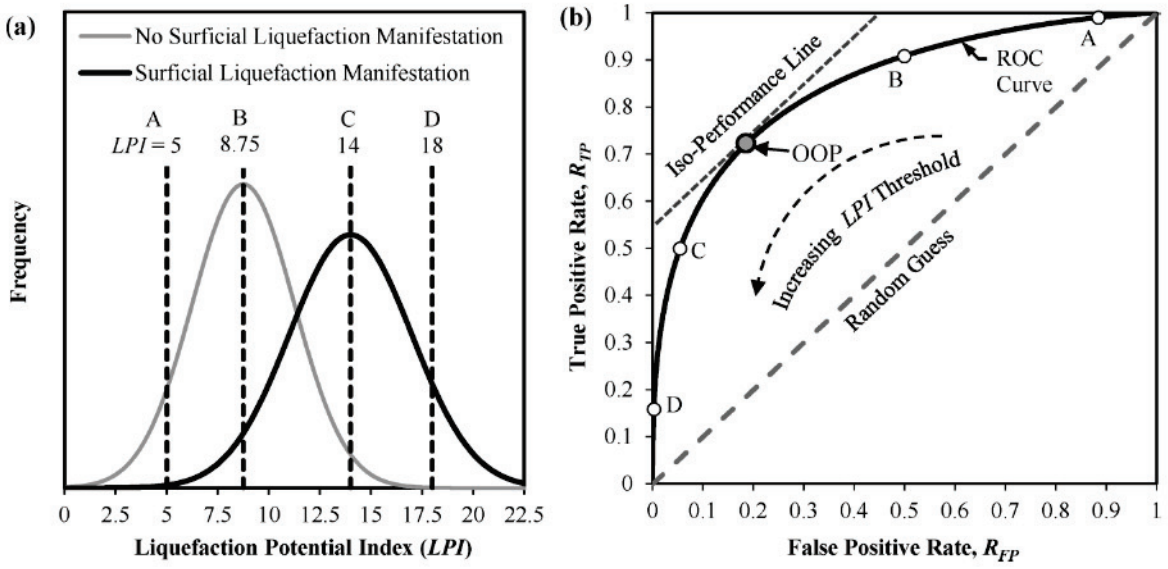

versus the false positive rate (R_{FP}) (i.e., surficial liquefaction manifestation is predicted but was not observed) for varying threshold values (e.g., MSI thresholds). Figure 2 shows a conceptual illustration of ROC analysis using LPI as an example. The distributions of LPI for positives and negatives is shown in Fig. 2*a*, and the relationship among the distributions, the threshold values, and the ROC curve is shown in Fig. 2*b*. For example, consider LPI = 8.75 is the threshold value that separates no surface manifestation from surface manifestation (i.e., if LPI > 8.75 liquefaction manifestations are predicted). From Fig. 2*a*, it can be seen that ~50% of the cases exhibiting no manifestation have LPI values greater than this threshold, while ~90% of the cases exhibiting manifestations have LPI values greater than this threshold. Accordingly, $R_{TP} \approx 90\%$ and $R_{FP} \approx 50\%$ for an LPI threshold value of 8.75 are plotted as Point B in Fig. 2*b*.

In ROC curve space, a diagnostic test that has no predictive ability (i.e., a random guess) results in an ROC curve that plots as a 1:1 line through the origin, which would be the case if the distributions of the no manifestation and manifestation cases have the same means and standard deviations (i.e., LPI has no ability to predict the occurrence of surface manifestations). In contrast, a diagnostic test that has a perfect predictive ability (i.e., a perfect model) plots along the left vertical and upper horizontal axes, connecting at the point (0,1) and indicates the existence of a threshold value that perfectly segregates the data set (e.g., all cases with observed surficial manifestation will have MSI above the threshold, and all cases with no observed surficial manifestation will have an MSI below the threshold). The area under the ROC curve (AUC) is statistically equivalent to the probability that cases with observed surficial liquefaction manifestation have higher computed MSI values than cases without observed surficial liquefaction manifestations (e.g., Fawcett 2005). Therefore, a larger AUC indicates better predictive capabilities. To put this into perspective, a random guess returns an AUC of 0.5, whereas a perfect model returns an AUC of 1. The optimum operating point (OOP) in an ROC analysis is defined as the threshold value (e.g., threshold LPI) that minimizes the rate of misprediction [i.e., $R_{FP} + (1 - R_{TP})$]. A contour of the quantity [$R_{FP} + (1 - R_{TP})$] plots as a straight line in the ROC space with slope of 1, also called an iso-performance line, as illustrated in Fig. 2*b*. As such, an iso-performance line is tangent to the ROC curve at the *OOP*.

Results and discussion

Relationship between MSI and severity of surficial liquefaction manifestation as a function of I_{c10}

For each MSI model, ROC analyses were performed on the entire data set as well as the subsets of the data set formed by grouping the data into different bins of I_{c10}. Similar to Maurer et al. (2015*b*), the data set was initially divided into two bins of I_{c10}: $I_{c10} < 2.05$ and $I_{c10} \geq 2.05$, where $I_c = 2.05$ is the I_c boundary between clean to silty sands and silty sands to sandy silts (Robertson and Wride 1998). Table 2 summarizes the ROC statistics (i.e., AUC and OOP values) for LPI, LPI_{Ish}, and LSN models, considering the entire data set as well as the two different subsets of I_{c10}. It can be observed that, for each MSI model, the OOP for the subset of cases with $I_{c10} \geq 2.05$ is significantly higher than that for the subset with $I_{c10} < 2.05$, indicating that the relationship between computed MSI and the severity of surficial liquefaction manifestation varies with I_{c10}. For example, for $I_{c10} < 2.05$, the threshold LPI for distinguishing cases with and without manifestation was found to be 3.7. In contrast, the threshold LPI for $I_{c10} \geq 2.05$ was found to be 7.5. Note that these threshold LPI values differ

Fig. 3. Example of I_c versus depth profiles from the CE data set that have I_{c10} falling in different ranges considered in this study: $I_{c10} < 1.7$; $1.7 \leq I_{c10} < 1.9$; $1.9 \leq I_{c10} < 2.1$; $2.1 \leq I_{c10} < 2.3$; and $I_{c10} \geq 2.3$.

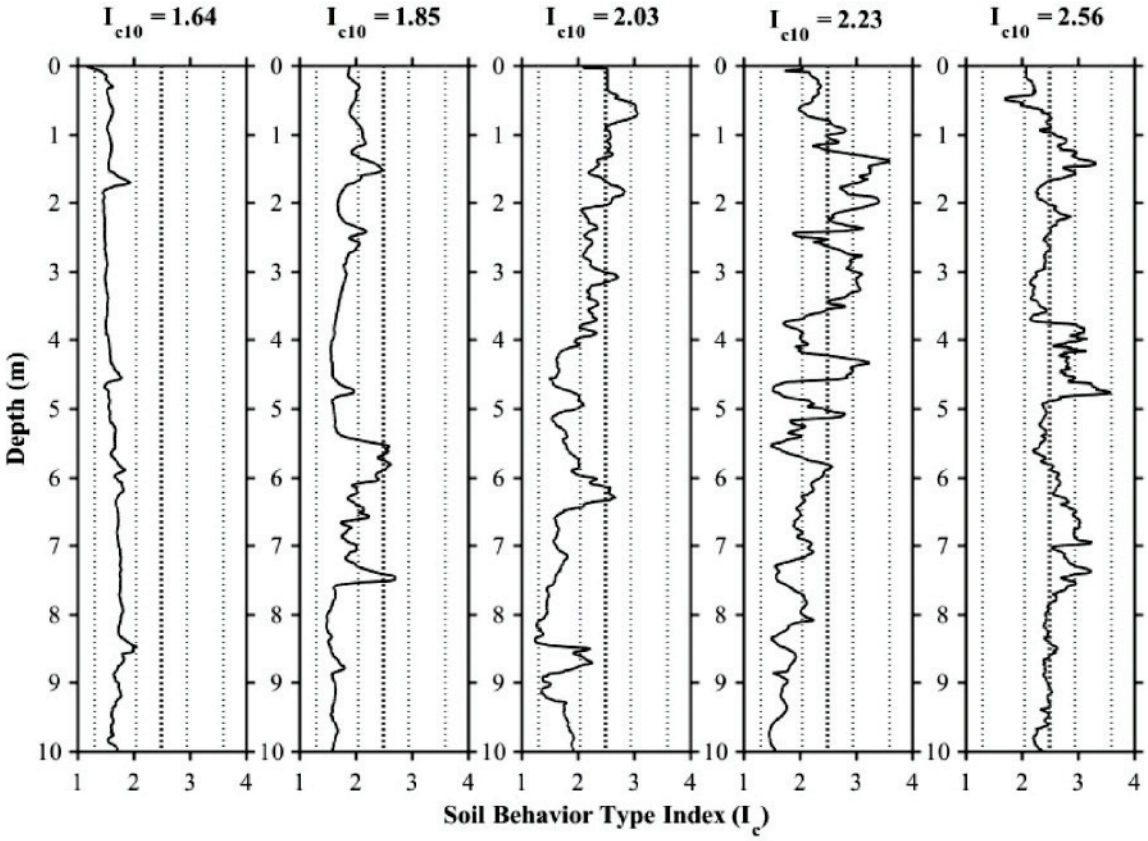

Table 2. Summary of ROC statistics on two subsets of I_{c10} for different MSI models.

	All I_{c10}		$I_{c10} < 2.05$		$I_{c10} \geq 2.05$	
MSI model	AUC	OOP	AUC	OOP	AUC	OOP
LPI	0.825	3.7	0.850	3.7	0.764	7.5
LPI_{Ish}	0.828	1.7	0.847	1.7	0.776	4.4
LSN	0.775	10	0.798	11	0.695	15

from those computed by Maurer et al. (2015*b*), who found the threshold LPI values for $I_{c10} < 2.05$ and $I_{c10} \geq 2.05$ to be 4.9 and 13, respectively. Potential factors for this discrepancy may include the use of a significantly larger number of case histories in the present study due to the addition of case histories from the 2016 Valentine's Day earthquake, updated estimates of PGAs for the 2011 Christchurch earthquake, and the I_c cutoff of 2.5 used herein versus the I_c cutoff of 2.6 used by Maurer et al. 2015*b*. Moreover, it was observed that, while the OOPs for $I_{c10} < 2.05$ were very similar to those obtained using the entire data set, the OOPs for $I_{c10} \geq 2.05$ were significantly higher. This is likely because the $I_{c10} < 2.05$ subset contains a significantly larger number of case histories than the $I_{c10} \geq 2.05$ subset (note that 75% of the CE case histories have $I_{c10} < 2.05$). Consequently, MSI thresholds that are derived using the entire data set may accurately predict the manifestations' severity for profiles having predominantly clean to silty sands but may over-predict the manifestation severity for profiles having predominantly silty to clayey soil mixtures. Furthermore, it may be observed that for each MSI model, the AUC values for $I_{c10} < 2.05$ are higher than those for $I_{c10} \geq 2.05$, indicating that each MSI model performs better at predicting the severity of surficial liquefaction manifestation for sites with $I_{c10} < 2.05$.

Similar analyses were performed using multiple finer bins of I_{c10} to evaluate the influence of I_{c10} on the predictive performance of the MSI models in greater resolution. For example, I_c versus depth profiles that have I_{c10} falling in five different ranges of I_{c10}: $I_{c10} < 1.7$; $1.7 \leq I_{c10} < 1.9$; $1.9 \leq I_{c10} < 2.1$; $2.1 \leq I_{c10} < 2.3$; and $I_{c10} \geq 2.3$ are shown in Fig. 3. Table 3 summarizes AUC and OOP values for these five different bins of I_{c10} for the LPI, LPI_{Ish}, and LSN models. In general, regardless of the MSI model used, the threshold MSI values were found to increase with increasing I_{c10}, which clearly indicates that for each MSI model the relationship between computed MSI and the severity of surficial liquefaction manifestation is I_{c10}-dependent. As such, for a given MSI value, the severity of manifestation decreases as I_{c10} increases. Therefore, I_{c10}-specific MSI thresholds may be employed to more accurately estimate the severity of surficial liquefaction manifestation at a given site. Furthermore, it can be observed that AUC values generally decrease with increasing I_{c10}, indicating that the predictive efficacy of the MSI models decreases with increasing I_{c10}.

Table 3. Summary of ROC statistics on multiple finer subsets of I_{c10} for different MSI models.

	$I_{c10} < 1.7$		$1.7 \le I_{c10} < 1.9$		$1.9 \le I_{c10} < 2.1$		$2.1 \le I_{c10} < 2.3$		$I_{c10} \ge 2.3$	
MSI model	AUC	OOP	AUC	OOP	AUC	OOP	AUC	OOP	AUC	OOP
LPI	0.860	2.3	0.855	3.9	0.808	7.5	0.798	7.1	0.791	8.8
LPI_{Ish}	0.850	0.5	0.857	1.7	0.814	3.1	0.804	3.9	0.737	4.4
LSN	0.812	8	0.801	13	0.745	13	0.718	15	0.659	15

Table 4. $P(S|\text{MSI}, I_{c10})$ model coefficients.

MSI model	B_0	B_1	B_2
LPI	−1.677	0.645	−0.206
LPI_{Ish}	−1.408	0.747	−0.233
LSN	−1.580	0.147	−0.033

The high I_{c10} soil profiles in Christchurch are generally found to be non-uniform with multiple interbedded layers of high-FC, high-plasticity soils. Different depositional environments from those in Christchurch could result in a profile having a given I_{c10} but a very different liquefaction manifestation response.

Probabilistic assessment of the severity of surficial liquefaction manifestation as a function of MSI and I_{c10}

As may be inferred from the results shown in the previous section, for any computed MSI, the probability of surficial liquefaction manifestation decreases as I_{c10} increases. As such, the probability of manifestation may be empirically estimated as a function of MSI and I_{c10} using a logistic regression approach. Logistic regression is a tool that can be used to estimate the probability that an event occurs given one or more predictor variables. Multiple liquefaction studies in the literature (e.g., Li et al. 2006*a*, *b*; Papathanassiou 2008; Chung and Rogers 2017; among others) have used logistic regression to estimate the probability of surface manifestation as a function of independent predictor variables (e.g., LPI).

The following empirical model was adopted in this study to express the probability of surficial liquefaction manifestation, S, as a function of MSI and I_{c10}:

$$P(S|\text{MSI}, I_{c10}) = \frac{1}{1 + e^{-[B_0 + (B_1 + B_2 \cdot I_{c10}) \cdot \text{MSI}]}} \quad (4)$$

where, B_0, B_1, and B_2 are the model coefficients that can be determined through regression analyses.

For each MSI model, B_0, B_1, and B_2 were obtained by performing generalized linear model regression (*glmfit*) with a *logit* link function in MATLAB (The Mathworks 2018), which is based on the maximum likelihood estimation approach (Baker 2011, 2015). Table 4 summarizes these model coefficients obtained using LPI, LPI_{Ish}, and LSN. Moreover, Figs. 4, 5, and 6 show plots of eq. 4 for different values of I_{c10}, using LPI, LPI_{Ish}, and LSN models, respectively. As such, the curves shown in Figs. 4–6 can be used to estimate the probability of surficial liquefaction manifestation for any computed MSI value as a function of I_{c10}. For example, using Fig. 4, for computed LPI = 10, the probability of surficial liquefaction manifestation would be ~84% for a site with $I_{c10} = 1.7$ but only ~31% for a site with $I_{c10} = 2.7$.

Fig. 4. Probability of surficial liquefaction manifestation as a function of LPI and I_{c10}.

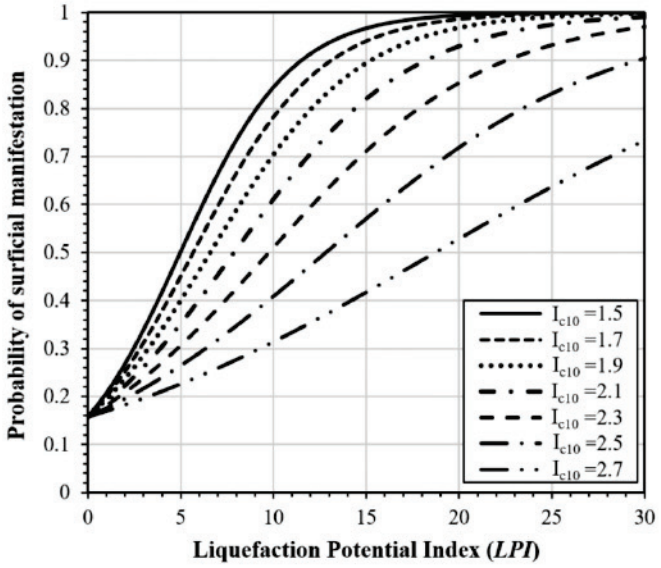

Fig. 5. Probability of surficial liquefaction manifestation as a function of LPI_{Ish} and I_{c10}.

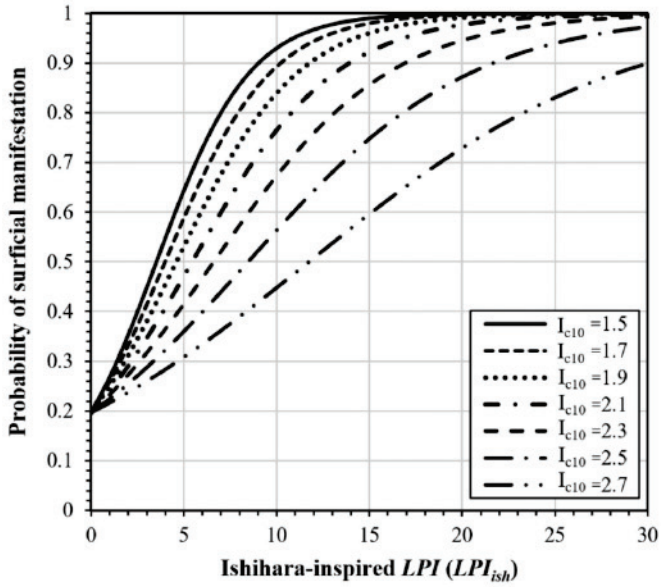

Fig. 6. Probability of surficial liquefaction manifestation as a function of LSN and I_{c10}.

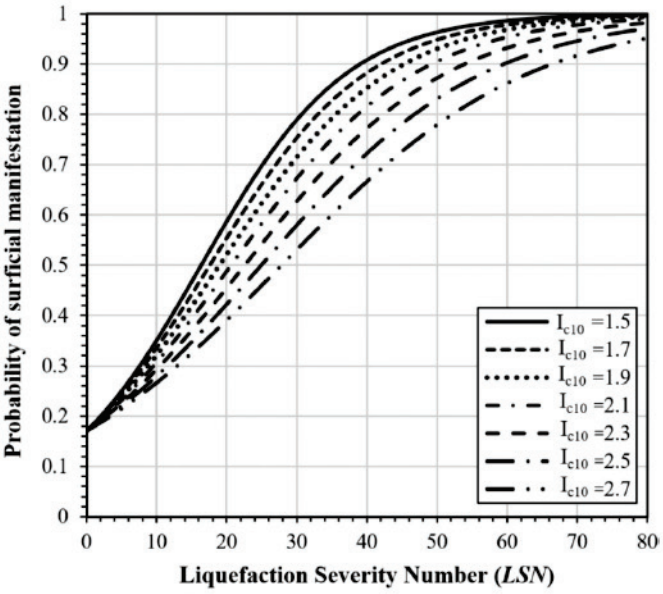

Note that in Figs. 4–6, the probability of surficial manifestation has low but nonzero values when the MSI are zero. This occurs because both LPI and LPI_{Ish} use a deterministic liquefaction triggering curve to obtain the factor of safety against liquefaction (eqs. 1 and 2). The deterministic curve corresponds to the probability of liquefaction triggering of about 15% (Boulanger and Idriss 2014); thus, while the FS may be greater than one, the probability of liquefaction triggering, and thus surface manifestation, is nonzero. Likewise, when LSN is used (Fig. 6; eq. 3), the expected value of ε_v is used to compute the LSN (Zhang et al. 2002). Thus, even for cases when the expected value of ε_v is zero, some low percentage of cases would be expected to exceed this value and thus retain the potential to exhibit surficial manifestation.

Using the CE data set, the predictive performance of the $P(S|MSI, I_{c10})$ model was compared with that of a probabilistic model expressed solely as a function of MSI [i.e., $P(S|MSI)$], to investigate whether including I_{c10} as a supplementary predictor variable to MSI provides any added benefit. The $P(S|MSI)$ model is defined as

$$P(S|MSI) = \frac{1}{1 + e^{-[C_0 + C_1 \cdot MSI]}} \quad (5)$$

where, C_0 and C_1 are the model coefficients and were determined through the regression approach described previously. The $P(S|MSI)$ coefficients obtained using LPI, LPI_{Ish}, and LSN are summarized in Table 5.

Two different performance metrics were used to compare the predictive efficacies of the $P(S|MSI, I_{c10})$ and $P(S|MSI)$ models: (a) AUC from ROC analysis and (b) Akaike information criterion (AIC) (Akaike 1973). While the AUC from ROC analysis is already discussed in a previous section, a brief description of the AIC is provided herein. AIC is a likelihood-based metric that can be used to select the best-performing model from a set of competing models fitted to the same data; the best-fitted model is the one that has the minimum AIC. AIC can be computed as

Table 5. P(S|MSI) model coefficients.

MSI model	C_0	C_1
LPI	−1.567	0.208
LPI_{Ish}	−1.358	0.259
LSN	−1.549	0.079

$$AIC = -2 \cdot \ln(L) + 2K \quad (6)$$

where L is the likelihood of producing the observed data for a given model and K is the number of model parameters.

Table 6 compares the AUC and AIC values for the $P(S|MSI, I_{c10})$ and $P(S|MSI)$ models derived using LPI, LPI_{Ish}, and LSN. It may be observed that regardless of the MSI model being used, the $P(S|MSI, I_{c10})$ model has a slightly higher AUC and a lower AIC than the $P(S|MSI)$ model, which is indicative of the improved performance of the former over the latter. Also shown in Table 6 are the increase in AUC and decrease in AIC values, designated as ΔAUC and ΔAIC, respectively. It can be observed that among the three MSI models considered in this study, ΔAUC and ΔAIC values follow the order: $LPI > LPI_{Ish} > LSN$. This indicates that inclusion of I_{c10} as the supplementary predictive variable was most effective for LPI and least effective for LSN. It should be noted, however, that the increase in AUC for each MSI is very small, indicating that the improvement in the model due to the inclusion of I_{c10} may not be statistically significant. This is likely because the CE data set is largely dominated by cases with lower I_{c10}. As mentioned previously, 75% of the CE case histories have $I_{c10} < 2.05$. As a result, the improvements in prediction due to the inclusion of I_{c10} is likely being averaged out among the different I_{c10} ranges.

Manifestation severity indices have been shown to correlate with the observed severity of surficial liquefaction manifestation, such that as MSI increases, the degree of manifestation severity increases. It is thus implied that the probability of surficial liquefaction manifestation would similarly correlate with the observed degree of manifestation severity. As such, the criteria based on probability of surficial liquefaction manifestation may be established to assess the severity of manifestation as a function of MSI and I_{c10}. For each MSI model, using CE case histories, ROC analyses were performed on the $P(S|MSI, I_{c10})$ values computed using eq. 4 to obtain optimum threshold probabilities distinguishing (a) cases with no manifestation from cases with any manifestation severity; (b) cases with no manifestation from cases with marginal manifestation; (c) cases with marginal manifestation from cases with moderate manifestation; and (d) cases with moderate manifestation from cases with severe manifestation. The MSI model-specific threshold probabilities of manifestation for different classes of manifestation severity are summarized in Table 7. Thus, instead of using I_{c10}-specific thresh-

Table 6. Comparison of AUC and AIC values between $P(S|\text{MSI}, I_{c10})$ and $P(S|\text{MSI})$ models.

	AUC			AIC		
MSI model	$P(S|\text{MSI}, I_{c10})$	$P(S|\text{MSI})$	ΔAUC	$P(S|\text{MSI}, I_{c10})$	$P(S|\text{MSI})$	ΔAIC
LPI	0.833	0.825	0.008	9741	10 054	313
LPI_{Ish}	0.834	0.828	0.006	10 080	10 275	195
LSN	0.777	0.775	0.002	11 175	11 222	47

Table 7. Optimum threshold probabilities for different severities of surficial liquefaction manifestation.

	Probability thresholds		
Manifestation severity	$P(S|\text{LPI}, I_{c10})$	$P(S|\text{LPI}_{\text{Ish}}, I_{c10})$	$P(S|\text{LSN}, I_{c10})$
Any manifestation	0.37	0.31	0.35
Marginal manifestation	0.25	0.28	0.31
Moderate manifestation	0.59	0.49	0.48
Severe manifestation	0.82	0.78	0.60

old MSI values as determined previously (e.g., Table 3), one set of probability-based criteria as shown in Table 7 may be used to assess the severity of the surficial liquefaction manifestation at any site.

Conclusions

Utilizing 9 631 high-quality liquefaction case histories from the M_w7.1 September 2010 Darfield earthquake, the M_w6.2 February 2011 Christchurch earthquake, and the M_w5.7 February 2016 Valentine's Day earthquake (i.e., CEs), this study investigated the predictive performances of LPI, LPI_{Ish}, and LSN models as a function of the CPT soil behavior type index (I_c) averaged over the upper 10 m of a soil profile (I_{c10}). In the context of this study, I_{c10} is used to infer the extent to which a profile contains high-FC, high-plasticity soils. It was shown that for each MSI model (1) the relationship between the computed MSI and severity of surficial liquefaction manifestation is I_{c10}-dependent, such that for a given MSI value, the severity of manifestation decreases as I_{c10} increases and (2) the predictive efficacy of the MSI model (i.e., the ability to segregate cases based on observed manifestation severity using MSI thresholds) decreases as I_{c10} increases. These findings suggest that I_{c10}-specific severity thresholds are needed to accurately estimate the severity of surficial liquefaction manifestations using an MSI model.

Additionally, using logistic regression, probabilistic models were proposed for evaluating the severity of surficial liquefaction manifestation as a function of MSI and I_{c10}. It was shown that the predictive efficacies of these models were higher than those of the models defined solely as a function of MSI, suggesting that including I_{c10} as an additional predictor variable improves the predictions of the liquefaction manifestation severity. Furthermore, optimum threshold probabilities for different severities of surficial liquefaction manifestation were determined by performing ROC analyses on the CE data set.

It should, however, be noted that the findings of this study are artifacts of inherent limitations in the existing MSI models to account for the influence of high-FC, high-plasticity soils on the occurrence and severity of surficial liquefaction manifestations. Given that the MSI models perform more poorly in profiles having high-FC, high-plasticity soils, the approaches presented herein are indirect ways to correct the predictions made by the existing MSI models. The ultimate goal of this research is to understand and incorporate the influence of high-FC, high-plasticity soils within the manifestation model itself. Finally, the findings from this study are entirely based on the case histories from Canterbury, New Zealand; their applicability to sites having stratigraphies that differ significantly from those used in this study is unknown.

List of symbols

AIC	Akaike information criterion—a likelihood-based metric that can be used to select the best-performing model from a set of competing models fitted to the same data; the best-fitted model is the one that has minimum AIC.
AUC	Area under the ROC curve—statistically equivalent to the probability that cases with observed surficial liquefaction manifestation have higher computed MSI values than cases without observed surficial liquefaction manifestations (e.g., Fawcett 2005). Therefore, a larger AUC indicates better predictive capabilities.
CEs	Canterbury earthquakes—specific to this study, the CEs consider the M_w7.1 September 2010 Darfield earthquake, the M_w6.2 February 2011 Christchurch earthquake, and the M_w5.7 February 2016 Valentine's Day earthquake
CPT	Cone penetration test—in situ test used in characterizing a soil profile

EQC	New Zealand Earthquake Commission
FC	Fines content—percentage by weight of the soil particles have an effective diameter less than 0.075 mm
FS	Factor of safety against liquefaction triggering—computed by a triggering model (e.g., Boulanger and Idriss 2014)
GWT	Depth to ground-water table
H_1	Thickness of the non-liquefied capping layer—associated with the Ishihara (1985) surficial liquefaction manifestation model and incorporated in the LPI_{Ish} MSI model
H_2	Thickness of the liquefied layer—associated with the Ishihara (1985) surficial liquefaction manifestation model and incorporated in the LPI_{Ish} MSI model
I_c	Soil behavior type index—an index computed from CPT data to estimate soil type
I_{c10}	Average I_c in the upper 10 m of a soil profile
LPI	Liquefaction potential index, a type of an MSI model
LPI_{Ish}	Ishihara LPI, a type of an MSI model
LSN	Liquefaction severity number, a type of an MSI model
OOP	Optimum operating point—associated with ROC analysis to define the threshold value (e.g., threshold LPI) that minimizes the rate of misprediction
PGA	Peak ground acceleration
MSI models	Manifestation severity index models
M_w	Moment magnitude
NZGD	New Zealand geotechnical database
q_{c1Ncs}	Normalized cone penetration resistance
ROC analysis	Receiver operator characteristic analysis—used to evaluate the performance of MSI models
R_{FP}	False positive rate—the rate of falsely predicting surficial liquefaction manifestations that occurred for a given MSI threshold value
R_{TP}	True positive rate—the rate of correctly predicting surficial liquefaction manifestations that occurred for a given MSI threshold value
SMS	Strong motion stations—instruments used to record earthquake motions
SPT	Standard penetration test—in situ test used in characterizing a soil profile
u2	Pore water pressure measurement made immediately behind the cone tip on a cone penetrometer during CPT testing
z	Depth
z_{max}	Maximum depth of liquefaction assumed to contribute to surficial liquefaction manifestations
ΔAUC	Increase in AUC as a result of including I_{c10} as a conditioning variable in the probability model
ΔAIC	Decrease in AIC as a result of including I_{c10} as a conditioning variable in the probability model
ε_v	Volumetric strain in soil due to post-liquefaction consolidation

Acknowledgements

The funding support for the research from which this paper is derived is gratefully acknowledged. However, any opinions, findings, and conclusions or recommendations expressed in this paper are those of the authors and do not necessarily reflect the views of the National Science Foundation, Pacific Earthquake Engineering Research Center, or the U.S. Geological Survey.

Article information

History dates

Received: 18 February 2022
Accepted: 30 August 2022
Accepted manuscript online: 15 November 2022
Version of record online: 5 April 2023

Data availability

Some or all data, models, or code that support the findings of this study are available from the corresponding author upon reasonable request.

Author information

Author ORCIDs

Russell A. Green https://orcid.org/0000-0002-5648-2331

Author Contributions

Conceptualization: B-WM, RAG
Data curation: B-WM, SVB
Formal analysis: SU, AR-M
Funding acquisition: RAG, AR-M
Investigation: SVB
Methodology: B-WM, RAG
Project administration: RAG, AR-M
Resources: SVB
Writing – original draft: SU
Writing – review & editing: B-WM, RAG, AR-M

Competing interests

The authors declare there are no competing interests.

Funding information

This research was funded by the National Science Foundation grants CMMI-1435494, CMMI-1724575, CMMI-1751216, CMMI-1825189, and CMMI-1937984, as well as the Pacific Earthquake Engineering Research Center grant 1132-NCTRBM and the U.S. Geological Survey award G18AP-00006.

Supplementary material

Supplementary data are available with the article at https://doi.org/10.1139/cgj-2022-0092.

References

Akaike, H. 1973. Information theory and an extension of the maximum likelihood principle. *In* Proceedings of the Second International Symposium on Information Theory, Tsahkadsor, Armenia, USSR, 2–8 September 1971, Akadémiai Kiadó, Budapest, Hungary. pp. 267–281.

Baker, J. 2011. Fitting fragility functions to structural analysis data using maximum likelihood estimation. Stanford University, Stanford, CA.

Baker, J. 2015. Efficient analytical fragility function fitting using dynamic structural analysis. Earthquake Spectra, **31**(1): 579–599. doi:10.1193/021113EQS025M.

Beyzaei, C.Z., Bray, J.D., Cubrinovski, M., Reimer, M., and Stringer, M. 2018. Laboratory-based characterization of shallow silty soils in southwest Christchurch. Soil Dynamics and Earthquake Engineering, **110**: 93–109. doi:10.1016/j.soildyn.2018.01.046.

Boulanger, R.W., and Idriss, I.M. 2014. CPT and SPT based liquefaction triggering procedures. Report No. UCD/CGM-14/01. Center for Geotechnical Modelling, Department of Civil and Environmental Engineering, UC Davis, CA, USA.

Boulanger, R.W., Moug, D.M., Munter, S.K., Price, A.B., and DeJong, J.T. 2016. Evaluating liquefaction and lateral spreading in interbedded sand, silt, and clay deposits using the cone penetrometer. Australian Geomechanics, **51**(4): 109–128.

Bradley, B.A. 2012. Strong ground motion characteristics observed in the 4 September 2010 Darfield, New Zealand earthquake. Soil Dynamics and Earthquake Engineering, **42**: 32–46. doi:10.1016/j.soildyn.2012.06.004.

Bradley, B.A. 2013a. A New Zealand-specific pseudo-spectral acceleration ground-motion prediction equation for active shallow crustal earthquakes based on foreign models. Bulletin of the Seismological Society of America, **103**(3): 1801–1822. doi:10.1785/0120120021.

Bradley, B.A. 2013b. Site-specific and spatially-distributed ground motion intensity estimation in the 2010–2011 christchurch earthquakes. Soil Dynamics and Earthquake Engineering, **48**: 35–47. doi:10.1016/j.soildyn.2013.01.027.

Bradley, B.A., and Cubrinovski, M. 2011. Near-source strong ground motions observed in the 22 February 2011 Christchurch earthquake. Seismological Research Letters, **82**: 853–865. doi:10.1785/gssrl.82.6.853.

Chung, J., and Rogers, J.D. 2011. Simplified method for spatial evaluation of liquefaction potential in the St. Louis area. Journal of Geotechnical and Geoenvironmental Engineering, **137**(5): 505–515. doi:10.1061/(ASCE)GT.1943-5606.0000450.

Chung, J., and Rogers, J.D. 2017. Deterministic and probabilistic assessment of liquefaction hazards using the liquefaction potential index and liquefaction reduction number. Journal of Geotechnical and Geoenvironmental Engineering, **143**(10): 0401703. doi:10.1061/(ASCE)GT.1943-5606.0001772.

Cubrinovski, M., Green, R.A., Allen, J., Ashford, S., Bowman, E., and Bradley, B. 2010. Geotechnical reconnaissance of the 2010 Darfield (Canterbury) earthquake. Bulletin of the New Zealand Society for Earthquake Engineering, **43**(4): 243–320. doi:10.5459/bnzsee.43.4.243-320.

Cubrinovski, M., Bray, J.D., Taylor, M., Giorgini, S., Bradley, B., Wotherspoon, L., and Zupan, J. 2011. Soil liquefaction effects in the central business district during the February 2011 Christchurch earthquake. Seismological Research Letters, **82**(6): 893–904. doi:10.1785/gssrl.82.6.893.

Cubrinovski, M., Rhodes, A., Ntritsos, N., and Van Ballegooy, S. 2019. System response of liquefiable deposits. Soil Dynamics and Earthquake Engineering, **124**: 212–229. doi:10.1016/j.soildyn.2018.05.013.

Fawcett, T. 2005. An introduction to ROC analysis. Pattern recognition letters, **27**(8): 861–874. doi:10.1016/j.patrec.2005.10.010.

Geyin, M., Maurer, B.W., Bradley, B.A., Green, R.A., and van Ballegooy, S. 2021. CPT-based liquefaction case histories compiled from three earthquakes in Canterbury, New Zealand. Earthquake Spectra, **37**(4): 2920–2945. doi:10.1177/8755293021996367.

Goda, K., and Hong, H.P. 2008. Spatial correlation of peak ground motions and response spectra. Bulletin of the Seismological Society of America, **98**(1): 354–465. doi:10.1785/0120070078.

Green, R.A., Allen, J., Wotherspoon, L., Cubrinovski, M., Bradley, B., Bradshaw, A., et al. 2011a. Performance of Levees (Stopbanks) during the 4 September 2010, M_w7.1 Darfield and 22 February 2011, M_w6.2 Christchurch, New Zealand earthquakes. Seismological Research Letters, **82**(6): 939–949. doi:10.1785/gssrl.82.6.939.

Green, R.A., Wood, C., Cox, B., Cubrinovski, M., Wotherspoon, L., Bradley, B., et al. 2011b. Use of DCP and SASW tests to evaluate liquefaction potential: predictions vs. observations during the recent New Zealand earthquakes. Seismological Research Letters, **82**(6): 927–938. doi:10.1785/gssrl.82.6.927.

Green, R.A., Cubrinovski, M., Cox, B., Wood, C., Wotherspoon, L., Bradley, B., and Maurer, B.W. 2014. Select liquefaction case histories from the 2010–2011 Canterbury earthquake sequence. Earthquake Spectra, **30**(1): 131–153. doi:10.1193/030713EQS066M.

Green, R.A., Maurer, B.W., Cubrinovski, M., and Bradley, B.A. 2015. Assessment of the relative predictive capabilities of CPT-based liquefaction evaluation procedures: lessons learned from the 2010–2011 Canterbury earthquake sequence. *In* Proceedings of the Sixth International Conference on Earthquake Geotechnical Engineering (6ICEGE), Christchurch, New Zealand, 2–4 November, 2015.

Green, R.A., Upadhyaya, S., Wood, C.M., Maurer, B.W., Cox, B.R., Wotherspoon, L., et al. 2017. Relative efficacy of CPT- versus Vs-based simplified liquefaction evaluation procedures. *In* Proceedings of the 19th International Conference on Soil Mechanics and Geotechnical Engineering, Seoul, Korea, 17–22 September 2017.

Green, R.A., Maurer, B.W., and van Ballegooy, S. 2018. The influence of the non-liquefied crust on the severity of surficial liquefaction manifestations: case history from the 2016 Valentine's Day earthquake in New Zealand. *In* Proceedings of the Geotechnical Earthquake Engineering and Soil Dynamics V (GEESD V), Liquefaction Triggering, Consequences, and Mitigation. *Edited by* S.J. Brandenberg and M.T. Manzari. ASCE Geotechnical Special Publication. pp. 21–32.

Ishihara, K. 1985. Stability of natural deposits during earthquakes. *In* Proceedings of the 11th International Conference on Soil Mechanics and Foundation Engineering. San Francisco, CA, USA. pp. 321–376.

Ishihara, K., and Yoshimine, M. 1992. Evaluation of settlements in sand deposits following liquefaction during earthquakes. Soils and Foundations, **32**(1): 173–188. doi:10.3208/sandf1972.32.173.

Iwasaki, T., Tatsuoka, F., Tokida, K., and Yasuda, S. 1978. A practical method for assessing soil liquefaction potential based on case studies at various sites in Japan. *In* Proceedings of the Second International Conference on Microzonation, San Francisco, CA, USA, 26 November 1978–1 December 1978. pp. 885–896.

Jeffries, M.G., and Davies, M.P. 1993. Use of CPTu to estimate equivalent SPT N_{60}. Geotechnical Testing Journal, **16**(4): 458–468.

Jia, M.C., and Wang, B.Y. 2012. Liquefaction testing of stratified sands interlayered with silt. Applied Mechanics and Materials, **256–259**: 116–119. doi:10.4028/www.scientific.net/AMM.256-259.116.

Juang, C.H., Yang, S.H., Yuan, H., and Fang, S.Y. 2005. Liquefaction in the Chi-Chi earthquake-effect of fines and capping non-liquefiable layers. Soils and Foundations, **45**(6): 89–101. doi:10.3208/sandf.45.89.

Lee, D.H., Ku, C.S., and Yuan, H. 2003. A study of liquefaction risk potential at Yuanlin, Taiwan. Engineering Geology, **71**(1): 97–117.

Li, D.K., Juang, C.H., and Andrus, R.D. 2006a. Estimation of liquefaction effect by means of liquefaction potential index. *In* Proceedings of the GeoShanghai International Conference 2006: Ground Modification and Seismic Mitigation. *Edited by* A. Porbaha, S. Shen, J. Wartman and J. Chai. ASCE Geotechnical Special Publication. pp. 359–364.

Li, D.K., Juang, C.H., and Andrus, R.D. 2006b. Liquefaction potential index: a critical assessment using probability concept. Journal of GeoEngineering, **1**(1): 11–24.

Maurer, B.W., Green, R.A., Cubrinovski, M., and Bradley, B.A. 2014. Evaluation of the liquefaction potential index for assessing liquefaction hazard in Christchurch, New Zealand. Journal of Geotechnical and Geoenvironmental Engineering, **140**(7): 04014032. doi:10.1061/(ASCE)GT.1943-5606.0001117.

Maurer, B.W., Green, R.A., and Taylor, O.S. 2015a. Moving towards an improved index for assessing liquefaction hazard: lessons from historical data. Soils and Foundations, **55**(4): 778–787. doi:10.1016/j.sandf.2015.06.010.

Maurer, B.W., Green, R.A., Cubrinovski, M., and Bradley, B. 2015b. Fines-content effects on liquefaction hazard evaluation for infrastructure during the 2010–2011 Canterbury, New Zealand earthquake sequence. Soil Dynamics and Earthquake Engineering, **76**: 58–68. doi:10.1016/j.soildyn.2014.10.028.

Maurer, B.W., Green, R.A., Cubrinovski, M., and Bradley, B. 2015c. Assessment of CPT-based methods for liquefaction evaluation in a liquefaction potential index framework. Géotechnique, **65**(5): 328–336. doi:10.1680/geot.SIP.15.P.007.

Maurer, B.W., Green, R.A., Cubrinovski, M., and Bradley, B. 2015d. Calibrating the liquefaction severity number (LSN) for varying misprediction economies: a case study in Christchurch, New Zealand. *In* Proceedings of the Sixth International Conference on Earthquake Geotechnical Engineering, Christchurch, New Zealand, 1–4 November 2015.

Maurer, B.W., Green, R.A., van Ballegooy, S., Bradley, B.A., and Upadhyaya, S. 2017a. Performance comparison of probabilistic and deterministic liquefaction triggering models for hazard assessment in 23 global earthquakes. *In* Geo-Risk 2017: reliability-based design and code developments. *Edited by* J. Huang, G.A. Fenton, L. Zhang and D.V. Griffiths. ASCE Geotechnical Special Publication. pp. 31–42.

Maurer, B.W., Green, R.A., van Ballegooy, S., and Wotherspoon, L. 2017b. Assessing liquefaction susceptibility using the CPT soil behavior type index. *In* Proceedings of the Third International Conference on Performance-Based Design in Earthquake Geotechnical Engineering (PBDIII), Vancouver, Canada, 16–19 July 2017.

Maurer, B.W., Green, R.A., van Ballegooy, S., and Wotherspoon, L. 2019. Development of region-specific soil behavior type index correlations for evaluating liquefaction hazard in Christchurch. Soil Dynamics and Earthquake Engineering, **117**: 96–105. doi:10.1016/j.soildyn.2018.04.059.

Oommen, T., Baise, L.G., and Vogel, R. 2010. Validation and application of empirical liquefaction models. Journal of Geotechnical and Geoenvironmental Engineering, **136**(12): 1618–1633. doi:10.1061/(ASCE)GT.1943-5606.0000395.

Ozutsumi, O., Sawada, S., Iai, S., Takeshima, Y., Sugiyama, W., and Shimazu, T. 2002. Effective stress analyses of liquefaction-induced deformation in river dikes. Soil Dynamics and Earthquake Engineering, **22**(9): 1075–1082. doi:10.1016/S0267-7261(02)00133-1.

Papathanassiou, G. 2008. LPI-based approach for calibrating the severity of liquefaction-induced failures and for assessing the probability of liquefaction surface evidence. Engineering Geology, **96**(1–2): 94–104. doi:10.1016/j.enggeo.2007.10.005.

Quigley, M.C., Bastin, S., and Bradley, B.A. 2013. Recurrent liquefaction in Christchurch, New Zealand, during the Canterbury earthquake sequence. Geology, **41**(4): 419–422. doi:10.1130/G33944.1.

Robertson, P.K., and Wride, C.E. 1998. Evaluating cyclic liquefaction potential using cone penetration test. Canadian Geotechnical Journal, **35**(3): 442–459. doi:10.1139/t98-017.

The Mathworks. 2018. MATLAB and statistics toolbox release 2018b. The Mathworks, Inc., Natick, MA, USA.

Upadhyaya, S., Maurer, B.W., Green, R.A., and Rodriguez-Marek, A. 2018. Effect of non-liquefiable high fines-content, high plasticity soils on liquefaction potential index (LPI) performance. *In* Geotechnical earthquake engineering and soil dynamics V: liquefaction triggering, consequences, and mitigation. *Edited by* S.J. Brandenberg and M.T. Manzari. ASCE Geotechnical Special Publication. pp. 191–198.

Upadhyaya, S., Green, R.A., Rodriguez-Marek, A., Maurer, B.W., Wotherspoon, L., Bradley, B.A., and Cubrinovski, M. 2019a. Influence of corrections to recorded peak ground accelerations due to liquefaction on predicted liquefaction response during the M_w 6.2, February 2011 Christchurch earthquake. *In* Proceedings of the 13th Australia New Zealand Conference on Geomechanics, Perth, Australia, 1–3 April 2019.

Upadhyaya, S., Green, R.A., Maurer, B.W., and Rodriguez-Marek, A. 2019b. Selecting factor of safety against liquefaction for design based on cost considerations. *In* Proceedings of the Seventh International Conference on Earthquake Geotechnical Engineering, Rome, Italy, 17–20 June 2019.

Upadhyaya, S., Green, R.A., Maurer, B.W., Rodriguez-Marek, A., and van Ballegooy, S. 2022. Limitations of surface liquefaction manifestation severity index models used in conjunction with simplified stress-based triggering models. Journal of Geotechnical and Geoenvironmental Engineering, **148**(3): 04021194. doi:10.1061/(ASCE)GT.1943-5606.0002725.

van Ballegooy, S., Malan, P.J., Jacka, M.E., Lacrosse, V.I.M.F., Leeves, J.R., Lyth, J.E., and Cowan, H. 2012. Methods for characterising effects of liquefaction in terms of damage severity. *In* Proceedings of the 15th World Conference on Earthquake Engineering (15 WCEE), Lisbon, Portugal, 24–28 September 2012.

van Ballegooy, S., Cox, S.C., Thurlow, C., Rutter, H.K., Reynolds, T., Harrington, G., et al. 2014a. Median water table elevation in Christchurch and surrounding area after the 4 September 2010 Darfield earthquake: version 2. GNS Science Report 2014/18.

van Ballegooy, S., Malan, P., Lacrosse, V., Jacka, M.E., Cubrinovski, M., Bray, J.D., et al. 2014b. Assessment of liquefaction-induced land damage for residential Christchurch. Earthquake Spectra, **30**(1): 31–55. doi:10.1193/031813EQS070M.

van Ballegooy, S., Green, R.A., Lees, J., Wentz, F., and Maurer, B.W. 2015. Assessment of various CPT based liquefaction severity index frameworks relative to the Ishihara 1985 H_1–H_2 boundary curves. Soil Dynamics and Earthquake Engineering, **79**(Part B): 347–364. doi:10.1016/j.soildyn.2015.08.015.

Wotherspoon, L.M, Orense, R.P, Bradley, B.A., Cox, B.R., Wood, C., and Green, R.A. 2014. Geotechnical Characterisation of Christchurch Strong Motion Stations, Earthquake Commission Biennial Grant Report; 2014, Project No. 12/629. Civil and Natural Resources Engineering, University of Canterbury, Christchurch, New Zealand.

Wotherspoon, L.M., Orense, R.P., Green, R.A., Bradley, B.A., Cox, B.R., and Wood, C.M. 2015. Assessment of liquefaction evaluation procedures and severity index frameworks at Christchurch strong motion stations. Soil Dynamics and Earthquake Engineering, **79**(Part B): 335–346. doi:10.1016/j.soildyn.2015.03.022.

Yost, K.M., Green, R.A., Upadhyaya, S., Maurer, B.W., Yerro-Colom, A., Martin, E., and Cooper, J. 2021. Assessment of the efficacies of correction procedures for multiple thin layer effects on cone penetration tests. Soil Dynamics and Earthquake Engineering, **144**: 106677. doi:10.1016/j.soildyn.2021.106677.

Yost, K.M., Yerro, A., Green, R.A., Martin, E., and Cooper, J. 2022. MPM modeling of cone penetration testing for multiple thin-layer effects in complex soil stratigraphy. Journal of Geotechnical and Geoenvironmental Engineering, **148**(2): 04021189. doi:10.1061/(ASCE)GT.1943-5606.0002730.

Zhang, G., Robertson, P.K., and Brachman, R.W.I. 2002. Estimating liquefaction-induced ground settlements from CPT for level ground. Canadian Geotechnical Journal, **39**(5): 1168–1180. doi:10.1139/t02-047.

Zhu, J., Baise, L.G., and Thompson, E.M. 2017. An updated geospatial liquefaction model for global application. Bulletin of the Seismological Society of America, **107**(3): 1365–1385. doi:10.1785/0120160198.

Zou, K.H. 2007. Receiver operating characteristic (ROC) literature research. Available from http://www.spl.harvard.edu/archive/spl-pre2007/pages/ppl/zou/roc.html [accessed 10 March 2016].